

Comparison of thermodynamics solvers in the polythermal ice sheet model SICOPOLIS

Ralf Greve^a, Heinz Blatter^{a,b}

^a*Institute of Low Temperature Science, Hokkaido University, Kita-19, Nishi-8, Kita-ku, Sapporo 060-0819, Japan*

^b*Institute for Atmospheric and Climate Science, ETH Zurich, Universitätstrasse 16, CH-8092 Zurich, Switzerland*

Corresponding author: Ralf Greve (greve@lowtem.hokudai.ac.jp)

Abstract

In order to model the thermal structure of polythermal ice sheets accurately, energy-conserving schemes and correct tracking of the cold-temperate transition surface (CTS) are necessary. We compare four different thermodynamics solvers in the ice sheet model SICOPOLIS. Two exist already, namely a two-layer polythermal scheme (POLY) and a single-phase cold-ice scheme (COLD), while the other two are newly-implemented, one-layer enthalpy schemes, namely a conventional scheme (ENTC) and a melting-CTS scheme (ENTM). The comparison uses scenarios of the EISMINT Phase 2 Simplified Geometry Experiments (Payne and others, 2000, *J. Glaciol.* 46, 227–238). The POLY scheme is used as a reference against which the performance of the other schemes is tested. Both the COLD scheme and the ENTC scheme fail to produce a continuous temperature gradient across the CTS, which is explicitly enforced by the ENTM scheme. ENTM is more precise than ENTC for determining the position of the CTS, while the performance of both schemes is good for the temperature/water-content profiles in the entire ice column. Therefore, the one-layer enthalpy schemes ENTC and ENTM are viable, easier implementable alternatives to the POLY scheme with its need to handle two different numerical domains for cold and temperate ice.

Keywords:

Ice sheet, Thermodynamics, Polythermal ice, Enthalpy method, Modeling

1. Introduction

Many glaciers and ice sheets are polythermal with disjoint cold and temperate domains, separated by the cold-temperate transition surface (CTS) (Blatter and Hutter, 1991). Both the Greenland and Antarctic ice sheets are Canadian-type polythermal, that is, they are mainly cold, except for distributed temperate layers at the base where strain heating is largest and where there is a geothermal contribution. It is thus important to model the thermodynamics of ice sheets correctly by distinguishing both domains and accounting for the transition conditions between them.

Various methods allow one to model the thermodynamic conditions in ice sheets. Thus far, SICOPOLIS (SImulation COde for POLythermal Ice Sheets; e.g., Greve, 1997b; Sato and Greve, 2012; Greve and Herzfeld, 2013; URL www.sicopolis.net) is the only three-dimensional ice sheet model that employs the *polythermal two-layer scheme*. In this method, the temperature and water-content fields in the two domains, cold and temperate ice, are computed on separate numerical domains, and the transition conditions at the CTS are used to track its position.

In most older ice sheet models (e.g., Huybrechts, 1990; Calov and Hutter, 1996; Payne and Dongelmans, 1997; Ritz and others, 1997), the *cold-ice method* was applied by resetting any computed temperatures that exceed the local pressure melting point to the local pressure melting point. While very simple, this means that energy is lost, and the water content in the temperate layer as well as the transition conditions at the CTS are ignored. The cold-ice method has, however, always been available in SICOPOLIS as an alternative to the polythermal two-layer method.

Aschwanden and others (2012) introduced a new, enthalpy-based approach for ice sheet thermodynamics. In this method, the thermodynamic fields of temperature in cold ice and water content in temperate ice are replaced by one common thermodynamic field, enthalpy¹, for both domains, and only one common field equation must be solved. However, the Stefan-type energy- and mass-flux matching conditions at the CTS, which are important for determining its position (Greve, 1997a), are not included explicitly in the formulation of the enthalpy scheme by Aschwanden and others (2012). Following the terminology of Blatter and Greve (2015), we refer to it as the *conventional one-layer enthalpy scheme*. This scheme has already been used

¹Owing to the incompressibility of ice, the enthalpy is identical to the internal energy.

in a number of ice sheet and glacier models (Brinkerhoff and Johnson, 2013; Golledge and others, 2013; Seroussi and others, 2013; Wilson and Flowers, 2013; Gilbert and others, 2014; Kleiner and others, 2015).

Two different conditions of the CTS must be distinguished. For melting conditions, cold ice flows across the CTS into the temperate layer, where water starts to accumulate due to strain heating along trajectories. The opposite situation, freezing conditions, occurs further downstream, where temperate ice flows across the CTS into the cold domain and the accumulated water content freezes out, releasing latent heat. For melting conditions, the temperature gradient and the water content are continuous across the CTS, while for freezing conditions, discontinuities of these quantities occur (Greve, 1997a). Since the CTS tends to be rather steep near the terminus, only a small area of the CTS is freezing, and therefore, in results of ice sheet models, freezing conditions usually only occur at very few isolated grid points (Greve, 1997b).

Kleiner and others (2015) tested the implementation of the conventional enthalpy scheme for a Canadian-type parallel-sided slab in one finite-difference and two finite-element ice sheet models (TIM-FD³, ISSM, COMice). Blatter and Greve (2015) compared the performance of four different versions of the enthalpy scheme for a parallel-sided slab with a custom-designed finite-difference program. Besides the conventional enthalpy scheme, they considered the *two-layer front-tracking enthalpy scheme* (an enthalpy version of the polythermal two-layer scheme mentioned above), the *one-layer melting-CTS enthalpy scheme* and the *one-layer freezing-CTS enthalpy scheme*. In the two latter schemes, explicit tracking of the melting or freezing CTS, based on the respective transition conditions at the CTS, has been added to the conventional enthalpy scheme. An important finding of these works was that the conventional one-layer enthalpy scheme can produce correct solutions for melting conditions at the CTS, provided that the numerical handling of the discontinuity of the enthalpy diffusivity across the CTS is done carefully. However, especially for finite-difference techniques, Blatter and Greve (2015) concluded that it is safer to use the one-layer melting-CTS enthalpy scheme, which enforces the transition conditions explicitly. For freezing conditions, the conventional one-layer enthalpy scheme fails because it cannot handle the associated discontinuities of the thermodynamic fields, and it is thus imperative to enforce the transition conditions at the CTS explicitly, as it is done in the one-layer freezing-CTS enthalpy scheme.

For this study, in addition to the previously existing polythermal two-

layer and cold-ice schemes, we have implemented the conventional one-layer enthalpy scheme and the one-layer melting-CTS enthalpy scheme in the SICOPOLIS model. For the reason given above, freezing conditions are not considered here. We attempt to test and verify these four schemes in SICOPOLIS, and in particular to test how the various schemes handle the melting CTS between cold and temperate ice for Canadian-type polythermal situations in ice sheets. Based on the results of Blatter and Greve (2015), we consider the polythermal two-layer scheme to be the most reliable method and thus use its results as benchmark solutions. In Sections 2 and 3 we give an overview of the theory of ice-sheet thermodynamics and describe the implementation of the various schemes in SICOPOLIS. Section 4 gives the set-up of the scenarios derived from the suite of EISMINT (European Ice Sheet Modeling INiTiative) Phase 2 Simplified Geometry Experiments (Payne and others, 2000) used for this study. In Section 5 we discuss the results, focusing on the simulated thickness of the temperate ice layer. Section 6 concludes the paper.

2. Outline of ice-sheet thermodynamics

2.1. Standard polythermal thermodynamics

The standard description of the thermodynamics of polythermal ice masses, for which we follow largely Greve (1997a), is based on the fields of absolute temperature T in cold ice and water content W in temperate ice. The evolution equation for temperature in cold ice is given by

$$\frac{\partial T}{\partial t} + \mathbf{v} \cdot \text{grad } T = \frac{1}{\rho c} \frac{\partial}{\partial z} \left(\kappa \frac{\partial T}{\partial z} \right) + \frac{Q}{\rho c}, \quad (1)$$

where t denotes time, z the vertical spatial coordinate, \mathbf{v} the three-dimensional velocity vector, $\rho = 910 \text{ kg m}^{-3}$ the ice density, κ the temperature-dependent heat conductivity of cold ice and c the temperature-dependent heat capacity of cold ice. Also, $Q = \text{tr}(\mathbf{t} \cdot \mathbf{D})$ is the volumetric strain heating, where \mathbf{t} is the Cauchy stress tensor, \mathbf{D} the strain-rate tensor, the middle dot (\cdot) denotes tensor contraction and tr the trace of a tensor. Horizontal diffusion terms have been neglected, which can be justified by scaling arguments making use of the shallowness of ice sheets (e.g. Greve and Blatter, 2009).

Similar to Eq. (1), the evolution equation for water content in temperate ice reads

$$\begin{aligned} \frac{\partial W}{\partial t} + \mathbf{v} \cdot \nabla W &= \frac{1}{\rho} \frac{\partial}{\partial z} \left(\nu \frac{\partial W}{\partial z} \right) + \frac{Q}{\rho L} \\ &\quad - \frac{c}{L} \left(\frac{\partial T_m}{\partial t} + \mathbf{v} \cdot \nabla T_m \right) + \frac{1}{\rho L} \frac{\partial}{\partial z} \left(\kappa \frac{\partial T_m}{\partial z} \right), \end{aligned} \quad (2)$$

where ν is the water diffusivity in temperate ice (assumed to be constant) and $L = 3.35 \times 10^5 \text{ J kg}^{-1}$ the latent heat of fusion. The very small terms in the second line of the equation arise from the fact that the temperature in temperate ice is not constant, but equal to the melting temperature T_m that depends on the local pressure p ,

$$T_m(p) = T_0 - \beta p, \quad (3)$$

where $T_0 = 273.15 \text{ K}$ is the reference temperature and $\beta = 9.8 \times 10^{-8} \text{ K Pa}^{-1}$ the Clausius-Clapeyron constant for air-saturated glacier ice (Hooke, 2005). As in Eq. (1), horizontal diffusion terms have been neglected in the evolution equation (2).

As already mentioned in Sect. 1, for melting conditions at the CTS, the temperature gradient and the water content must be continuous across the CTS (Greve, 1997a). If we mark values at the cold side of the CTS by plus (+) superscripts, values at the temperate side by minus (−) superscripts, and denote the normal unit vector pointing into the cold side by \mathbf{n} , this reads

$$\nabla T^+ \cdot \mathbf{n} = \nabla T_m^- \cdot \mathbf{n} \quad (4)$$

and

$$W^+ = W^- = 0. \quad (5)$$

For freezing conditions, the situation is more complicated in that the temperature gradient and the water content are in general discontinuous across the CTS (Blatter and Hutter, 1991; Greve, 1997a). However, as already mentioned in Sect. 1, this situation usually occurs only on very small parts of the CTS, and therefore we do not consider freezing conditions in this study.

At the ice surface, we prescribe the surface temperature as a Dirichlet-type boundary condition. At the ice base, three different cases must be distinguished. For a cold base, the geothermal heat flux determines the

normal derivative of the temperature (Neumann-type boundary condition). For a temperate base with no temperate ice layer above, the temperature is equal to the pressure melting point. For a temperate base with a temperate ice layer above, in addition to that, a boundary condition for the basal water content is required (unless the water diffusivity ν is neglected). In order to influence the solution as little as possible, we choose the Neumann-type zero-flux condition $\partial W/\partial z = 0$.

In order to prevent the water content in temperate ice from rising to unreasonable levels due to the accumulated strain heating, a drainage model is required. We have kept the simple formulation previously implemented in SICOPOLIS, which assumes that any water exceeding the prescribed threshold of $W_{\max} = 0.01$ ($= 1\%$) is drained instantaneously. The transport mechanism to the ice base remains unmodeled; however, the amount of drained water is added to the computed basal melt rate, and thus accounted for in the computation of the vertical velocity and the evolution of the ice thickness.

2.2. Enthalpy method

As an alternative to the polythermal thermodynamics outlined in Sect. 2.1, Aschwanden and others (2012) introduced the enthalpy method. Its strength is that it combines the temperature and water content into a single thermodynamic field, the specific enthalpy, for which a single field equation holds.

The specific enthalpy h of ice at absolute temperature T and water content W is given by

$$h(T, W) = \int_{T_0}^T c(\tilde{T}) d\tilde{T} + LW. \quad (6)$$

Inversely, the temperature and water content are not unique functions of the enthalpy because of the dependence of the melting temperature on the pressure (Eq. (3)). We denote the inverse of Eq. (6) for zero water content ($W = 0$) by $T(h)$ and the enthalpy of ice at the melting point for zero water content by h_m ,

$$h_m(p) = h(T_m(p), W=0) = \int_{T_0}^{T_m(p)} c(\tilde{T}) d\tilde{T}. \quad (7)$$

The temperature and water content can then be obtained by

$$T(h, p) = \begin{cases} T(h), & h < h_m(p), \\ T_m(p), & h \geq h_m(p), \end{cases} \quad (8)$$

$$W(h, p) = \begin{cases} 0, & h < h_m(p), \\ L^{-1}(h - h_m(p)), & h \geq h_m(p). \end{cases} \quad (9)$$

The balance equation for enthalpy reads

$$\frac{\partial h}{\partial t} + \mathbf{v} \cdot \nabla h = \frac{\partial}{\partial z} \left(k_{c,t} \frac{\partial h}{\partial z} \right) + \frac{Q}{\rho}, \quad (10)$$

where

$$k_{c,t} = \begin{cases} k_c = \frac{\kappa}{\rho c}, & h < h_m(p), \\ k_t = \frac{\nu}{\rho}, & h \geq h_m(p) \end{cases} \quad (11)$$

are the enthalpy diffusivities in cold (subscript c) and temperate (subscript t) ice, respectively. Like in Eqs. (1) and (2), horizontal diffusion terms have been neglected in Eq. (10), while vertical diffusion is present in both cold and temperate ice.

The transition conditions for a melting CTS, Eqs. (4) and (5), transform into physically equivalent enthalpy conditions. Inserting Eq. (5) in Eq. (6) and considering that the temperature on both sides of the CTS is equal to the pressure melting point T_m yields the continuity of the enthalpy,

$$h^+ = h^- = h_m. \quad (12)$$

On the cold side of the CTS, $W = 0$ holds everywhere, so that differentiating Eq. (6) yields $\nabla h^+ = c(T_m) \nabla T^+$. On the temperate side, differentiating Eq. (7) yields $\nabla h_m^- = c(T_m) \nabla T_m^-$. Hence, the enthalpy form of Eq. (4) is

$$\nabla h^+ \cdot \mathbf{n} = \nabla h_m^- \cdot \mathbf{n}, \quad (13)$$

which expresses the continuity of the sensible heat flux. Note that the enthalpy gradient across the CTS is in general discontinuous ($\nabla h^+ \cdot \mathbf{n} > \nabla h_m^- \cdot \mathbf{n}$) because the enthalpy in the temperate ice layer becomes larger than h_m away from the CTS due to the increasing water content.

For freezing conditions, in general the enthalpy and the sensible heat flux are discontinuous ($h^+ < h^-$, $\nabla h^+ \cdot \mathbf{n} < \nabla h_m^- \cdot \mathbf{n}$). The exact form of the transition conditions shall not be given here.

By employing Eq. (6), the boundary conditions for the ice surface and base, as well as the simple drainage model, given in the last two paragraphs of Sect. 2.1 translate readily to the enthalpy formulation. However, for a

temperate base with a temperate ice layer above, instead of the zero-flux condition for the water content $\partial W/\partial z = 0$ we use the zero flux condition for the enthalpy $\partial h/\partial z = 0$. Since the temperature in temperate ice is not constant (Eq. (3)), these conditions are not equivalent, but the difference is small and both conditions are ad-hoc anyway, so that this is acceptable for the sake of simplicity.

3. Thermodynamics solvers in SICOPOLIS

Previous versions of SICOPOLIS (3.1 and older) contained two different options for dealing with ice-sheet thermodynamics. These are the polythermal two-layer scheme and the cold-ice scheme. Here, we added two more options based on the enthalpy method and the schemes described by Blatter and Greve (2015), namely the conventional one-layer enthalpy scheme and the one-layer melting-CTS enthalpy scheme. Freezing conditions at the CTS are not considered.

Blatter and Greve (2015) elaborated the schemes only for a one-dimensional problem (parallel-sided slab). Here, we extended them to three dimensions. SICOPOLIS uses terrain-following (“sigma”) coordinates, and the transformation to these coordinates produces extra terms (e.g., Greve and Blatter, 2009, Sect. 5.7.1). However, since horizontal diffusion has been neglected in Eq. (10), even in the transformed coordinates no mixing of horizontal and vertical derivatives of the enthalpy h occurs. This allows employing an implicit discretization scheme for the vertical derivatives and an explicit scheme for the horizontal derivatives in the same way as for the temperature and water-content equations (1) and (2) (Greve, 1997b). Thus, the numerical solution for each vertical profile is similar to the solution of the one-dimensional problem by an implicit scheme, and the horizontal advection terms of the three-dimensional equation play the role of additional, explicitly discretized source terms.

3.1. Polythermal two-layer scheme (POLY)

The polythermal two-layer scheme (scheme code: POLY) is the most sophisticated, but also the most complex method to simulate polythermal ice masses. It splits the computational domain numerically into two distinct layers of cold and temperate ice, and solves the evolution equations for temperature in cold ice (Eq. (1)) and water content in temperate ice (Eq. (2)) on two different grids (Blatter and Hutter, 1991; Greve, 1997a; Pettersson and

others, 2007). In this method, the CTS is fixed with the lower and upper boundaries of the cold and temperate domains, respectively, and thus can be tracked very precisely with the transition condition at the CTS.

The method works for both melting and freezing conditions at the CTS; in particular, it can cope with the discontinuities of the temperature gradient and the water content that accompany freezing conditions. It is implemented in SICOPOLIS as an iterative trial-and-error procedure. For each time step and each ice column for which an internal CTS is detected, the temperature problem for the upper (cold-ice) region and the water-content problem for the lower (temperate-ice) region are solved repeatedly with different test positions of the CTS until all boundary and transition conditions are fulfilled. This is discussed in more detail by Greve (1997b, last paragraph of section 2). For the simulations discussed in this study, we disregard freezing conditions and apply the POLY scheme only for assumed melting conditions at the CTS. The ability to turn off the freezing conditions is a newly-implemented option for the POLY scheme.

3.2. Cold-ice scheme (COLD)

The cold-ice scheme (scheme code: COLD) is the most simple, yet physically incorrect way to deal with polythermal conditions in ice sheets. SICOPOLIS applies the COLD scheme by solving the temperature equation (1) for the entire domain and resetting any temperatures T exceeding the local pressure melting point T_m (Eq. (3)) to $T = T_m$. The excess heat of the temperate layer becomes lost, so that the scheme does not conserve energy.

3.3. Conventional one-layer enthalpy scheme (ENTC)

The conventional one-layer enthalpy scheme (scheme code: ENTC) corresponds to the enthalpy method by Aschwanden and others (2012). The enthalpy equation (10) is solved for the entire polythermal domain on a single numerical grid, and the CTS is diagnostically determined as the uppermost grid point of the temperate layer, that is, the uppermost grid point for which $h \geq h_m$ holds. The transition conditions at the CTS, Eqs. (12) and (13) for melting conditions or their more complicated counterparts for freezing conditions, are not enforced explicitly.

3.4. One-layer melting-CTS enthalpy scheme (ENTM)

The one-layer melting-CTS enthalpy scheme (scheme code: ENTM) by Blatter and Greve (2015) differs from the conventional one-layer enthalpy

(ENTC) scheme in that the continuity condition (13) at a melting CTS is enforced explicitly. This is achieved for each vertical column possessing an internal CTS (that is, a non-vanishing thickness of temperate ice at the base) in two steps. In a predictor step, the enthalpy profile is computed for the entire vertical column like in the ENTC scheme. The CTS is then positioned at the uppermost point in the temperate layer. In a corrector step, the enthalpy profile in the upper, cold layer only is recomputed by using condition (13) as lower boundary condition. The updated enthalpy profile then consists of the predictor step for the temperate layer and the corrector step for the cold layer. For the technical details of the scheme see Blatter and Greve (2015).

The implementation of both the ENTC and the ENTM scheme in SICOPOLIS has the same topological restriction as the POLY scheme. It only allows for Canadian-type polythermal conditions, that is, only one CTS can exist in each column of ice, and the cold layer is always situated above the temperate layer. However, this is not a fundamental restriction for the enthalpy schemes. In principle, they also allow dealing with more complex and/or changing topologies such as temperate ice at the surface, prescribed water content instead of prescribed temperature as a boundary condition at the surface, bubbles of temperate ice within cold ice etc.

4. Experiment set-up

We tested the four different schemes described in Sect. 3 with modified versions of the EISMINT Phase 2 Simplified Geometry Experiments A and H as defined in Payne and others (2000). The computational domain in the horizontal plane is a square of 1500 by 1500 km, spanned by the Cartesian coordinates $x = 0 \dots 1500$ km, $y = 0 \dots 1500$ km. The numerical values of the dynamical and thermodynamical parameters are given in Payne and others (2000) (see also Sect. 2). The experiments were performed using SICOPOLIS version 3.2-dev (revision 471) with three different combinations of horizontal grid resolution Δx ($= \Delta y$) and time step Δt , namely $(\Delta x, \Delta t) = (10 \text{ km}, 2 \text{ a})$, $(5 \text{ km}, 2 \text{ a})$ and $(10 \text{ km}, 20 \text{ a})$. For the 10-km resolution, this leads to 151×151 grid points (indices $i = 0 \dots 150$, $j = 0 \dots 150$) in the horizontal domain, while for the 5-km resolution the domain is covered by 301×301 grid points. The standard vertical resolution is 81 grid points in the upper domain (terrain-following vertical coordinate $\zeta_c = 0 \dots 1$, index $k_c = 0 \dots 80$) and, for the POLY scheme, 11 grid points in the lower domain

(terrain-following vertical coordinate $\zeta_t = 0 \dots 1$, index $k_t = 0 \dots 10$). For the other three schemes, the lower domain is not used. For the (10 km, 2 a) combination, we also consider a five times higher vertical resolution (abbreviated as “hvr”) with 401 grid points in the upper and 51 grid points in the lower domain.

Both the heat capacity c and the heat conductivity κ depend significantly on temperature (e.g. Greve and Blatter, 2009). The implementation of all thermodynamics schemes in SICOPOLIS accounts for that possibility by allowing both quantities to vary in space and time. This is particularly relevant for discretizing the vertical diffusion terms in Eqs. (1), (2) and (10) that contain κ within $\partial/\partial z$ terms. However, in the EISMINT set-up used here the values are taken as constants, $c = 2009 \text{ J kg}^{-1}\text{K}^{-1}$ and $\kappa = 2.1 \text{ W m}^{-1}\text{K}^{-1}$ (Payne and others, 2000). The diffusive flux in the temperate layer is likely very small for small water contents; however, virtually no information on the value of the water diffusivity ν is available. In SICOPOLIS, a value of $\nu = 10^{-6} \text{ kg m}^{-1}\text{s}^{-1}$ is implemented for reasons of numerical stability rather than for physical reasons. This leads to $k_t = \nu/\rho \approx 1.1 \times 10^{-9} \text{ m}^2\text{s}^{-1}$, while $k_c = \kappa/(\rho c) \approx 1.1 \times 10^{-6} \text{ m}^2\text{s}^{-1}$, thus a three orders of magnitude difference.

4.1. EISMINT experiment A1

The experiment is started with no-ice conditions and runs for 200 ka to reach a steady state. The ice sheet rests on a flat, rigid base (no isostatic adjustment). The boundary conditions are circularly symmetric with respect to the center of the domain. The prescribed surface temperature increases linearly with distance from the center, with a minimum value of 238.15 K at the center (summit) and a horizontal gradient of $1.67 \times 10^{-2} \text{ K km}^{-1}$. Similarly, the surface mass balance is prescribed by a piece-wise linear function with a maximum accumulation rate of 0.5 m a^{-1} in the interior of the ice sheet (from the center to 400 km away from the center), and a horizontal gradient of $-10^{-2} \text{ m a}^{-1}\text{km}^{-1}$ beyond that, which leads to an equilibrium line 450 km from the center and an ablation zone further out. With these assumptions, the evolving ice sheet thickness does not feed back on the surface mass balance. At the ice base, no-slip conditions are assumed everywhere, and the geothermal heat flux is 42 mW m^{-2} .

There are two differences compared to the original EISMINT experiment A. The first one is the higher horizontal resolution; we use 10 and 5 km (see above) compared to the original 25 km. The second one is that, following Lliboutry and Duval (1985), we employ a water-content-dependent rate factor

A_t for temperate ice,

$$A_t(W) = A_{0^\circ\text{C}} \times (1 + 1.8125 W[\%]), \quad (14)$$

where $A_{0^\circ\text{C}} = 4.529 \times 10^{-24} \text{ s}^{-1} \text{ Pa}^{-3}$ is the rate factor for 0°C (relative to pressure melting) that results from the original EISMINT set-up.

4.2. EISMINT experiment A2

The set-up of experiment A2 is essentially the same as that of experiment A1; however, the water-content-dependent rate factor (14) is not used. Instead, the original EISMINT set-up is used, which only considers the dependence of the rate factor on temperature. Physically, this means that the lubrication effect of the near-basal temperate ice due to its water content is ignored.

4.3. EISMINT experiment H1

Experiment H1 replaces the no-slip condition of A1 by basal sliding. Otherwise, the set-up is the same. The sliding law is most simple and relates the sliding velocity linearly to the basal drag. In the original experiment H, the sliding parameter has the value $10^{-3} \text{ m a}^{-1} \text{ Pa}^{-1}$. However, this does not produce any basal temperate layers except for the COLD scheme due to the strong, downward advection of cold surface ice. Since we want to focus on the temperate ice, we decided to use a modified set-up, with the sliding parameter reduced by a factor 10 to the value $C_b^0 = 10^{-4} \text{ m a}^{-1} \text{ Pa}^{-1}$.

Further, in the EISMINT set-up, basal sliding is assumed to occur whenever the ice base is at the pressure melting point, while for a cold base no-slip conditions prevail. However, when used with the shallow ice approximation (that is employed by SICOPOLIS), this binary switch is known to produce a singularity of the vertical velocity field that prohibits proper convergence of the numerical solution (Bueler and Brown, 2009). In order to circumvent this problem, we regularize the transition by allowing for sub-melt sliding in the form by Greve (2005) (originally proposed by Hindmarsh and Le Meur (2001)). The sliding parameter C_b depends on the basal temperature T'_b (in $^\circ\text{C}$, relative to pressure melting) via

$$C_b = C_b^0 \exp(T'_b/\gamma), \quad (15)$$

where $\gamma = 1^\circ\text{C}$ is the sub-melt-sliding parameter. Equation (15) has the effect that, rather than stopping abruptly, basal sliding decays exponentially as the basal temperature falls below the pressure melting point.

5. Results

For experiment A1, run with the polythermal two-layer (POLY) scheme and the parameters $\Delta x = 10$ km, $\Delta t = 2$ a, Fig. 1 depicts the simulated steady-state ice thickness (= surface topography) at the end of the simulation ($t = 200$ ka). The ice sheet reaches a volume of 2.109×10^6 km³, covers an area of 1.046×10^6 km² and reaches a maximum thickness of 3.687 km. The melt fraction (fraction of basal ice at the pressure melting point) is 67.5%.

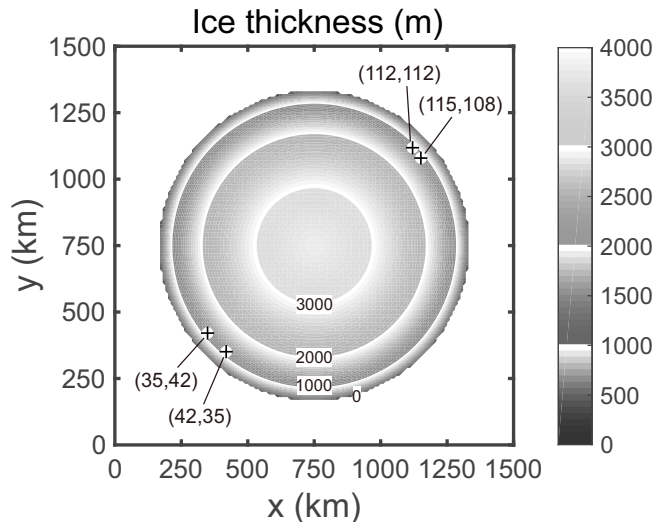


Figure 1: EISMINT experiment A1: Simulated ice thickness (= surface topography) after 200 ka model time. Polythermal two-layer (POLY) scheme, grid resolution $\Delta x = 10$ km, time step $\Delta t = 2$ a. The positions of the four profiles shown in Fig. 2 are marked by their respective grid indices (i, j) . Within grid resolution, they are at the same distance from the center [(35,42), (42,35) and (115,108) 518.6 km away, (112,112) 523.3 km away].

For the same set-up, Fig. 2 shows four steady-state temperature profiles (at $t = 200$ ka) in the bottom-most 80 m of the ice. They are all located near the margin, ~ 520 km away from the center, where the largest thicknesses of the temperate layer occur. The positions of the profiles are indicated in Fig. 1. The profiles show the typical patterns of the four different schemes concerning the position of the CTS, how they match the transition conditions at the CTS and the influence of the discrete grid. Evidently, the POLY scheme produces the best solutions. The computed temperature profiles are

both continuous and smooth across the CTS, thus fulfilling the transitions conditions for melting conditions. This justifies our decision (already stated in the last paragraph of the introduction) to use the solutions computed with the POLY scheme as a reference to assess the performance of the other three schemes.

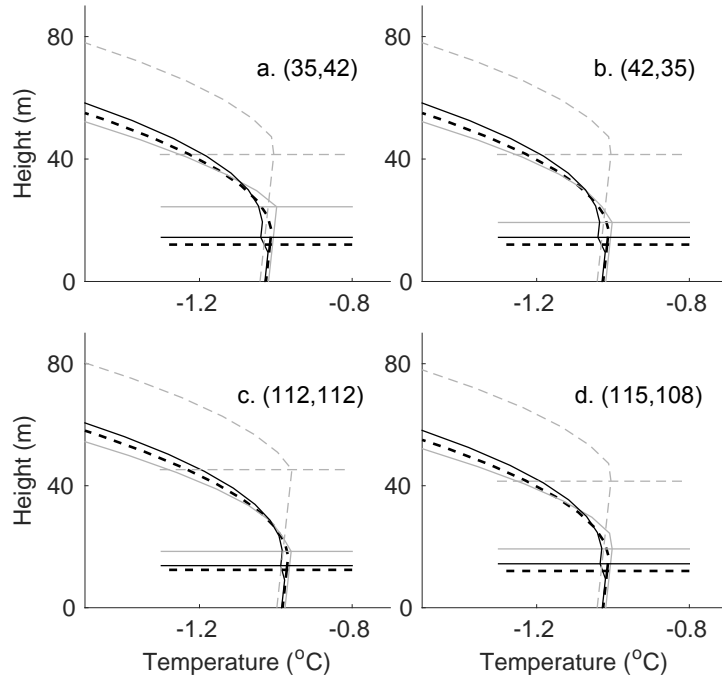


Figure 2: EISMINT experiment A1: Vertical temperature profiles after 200 ka model time at four different positions near the diagonal symmetry axis of the ice sheet (marked by their respective grid indices (i, j) , see Fig. 1) in the zone of maximum thickness of the temperate layer. Grid resolution $\Delta x = 10$ km, time step $\Delta t = 2$ a. Black dashed: POLY scheme, gray dashed: COLD scheme, gray solid: ENTC scheme, black solid: ENTM scheme (see Sect. 3 for the scheme codes). The horizontal lines mark the CTS positions.

In the depicted four profiles, the COLD scheme overestimates the thickness of the temperate layer by a factor ~ 3.5 . This overestimation, which was already reported by Greve (1997b) for simulations of the Greenland ice sheet with the SICOPOLIS model, is paralleled by a violation of the transition condition (4): the temperature gradient across the CTS is not continuous (most pronounced in Fig. 2c).

The profiles obtained with the ENTC scheme also overestimate the thickness of the temperate layer, but to a lesser extent than the cold-ice method (factor $\sim 1.5 - 2$). Like for the COLD scheme, the transition condition (4) (or its equivalent enthalpy form, Eq. (13)) is not fulfilled at the CTS.

The temperate layer thicknesses found by the ENTM scheme are most similar to those produced by the POLY scheme. Further, the temperature profiles all show a continuous gradient across the CTS, that is, they fulfill the transition condition (4) (or the equivalent form (13)). However, the price to pay for its enforcement by the corrector step described in Sect. 3.4 is that the temperature itself shows a slight discontinuity of $\sim 0.02 - 0.03$ K. Ultimately, this results from the fact that, in a one-layer scheme, the positioning of the CTS is naturally limited by the grid resolution (while, in the two-layer POLY scheme, arbitrary precision can be achieved).

Comparing the temperature profiles in the cold-ice layer above the CTS shows that, despite the differences in the position of the CTS, the results produced by the POLY, ENTM and ENTC schemes are very close to each other. In detail, for all four profiles, the ENTM scheme is slightly warmer, while the ENTC scheme is slightly colder than the POLY scheme. By contrast, the COLD scheme produces notably (~ 0.4 K) higher temperatures.

For the POLY, ENTM and ENTC schemes, the majority of grid points within the temperate layer reach a water content of $W = W_{\max} = 0.01$, which is the prescribed threshold value of the simple drainage model (see the last paragraph of Sect. 2.1). Therefore, we refrain from showing the water content in a separate figure. The COLD scheme is an exception because it does not account for any water content; in other words, the water content is zero everywhere.

In the following, we focus on the volume and thickness distribution of the simulated temperate ice layers. This is because (a) the thermal conditions at and near the ice base (where most of the shearing takes place) are most relevant for ice flow, and (b) within the temperate ice, the water content usually reaches the value $W_{\max} = 0.01$ (see above). Figure 3 shows the evolution of the temperate ice volume for experiment A1, run with the four thermodynamics schemes, the grid spacing $\Delta x = 10$ km, the two time steps $\Delta t = 20$ a and 2 a, and both the standard and high vertical resolution (“hvr”, see Sect. 4) set-ups. The period is limited to the first 20 ka of the total 200 ka model time, during which most of the changes take place.

For all shown cases, the temperate ice volume starts forming 6 - 7 ka after the initiation of the ice-sheet build-up, goes through a weak maximum and

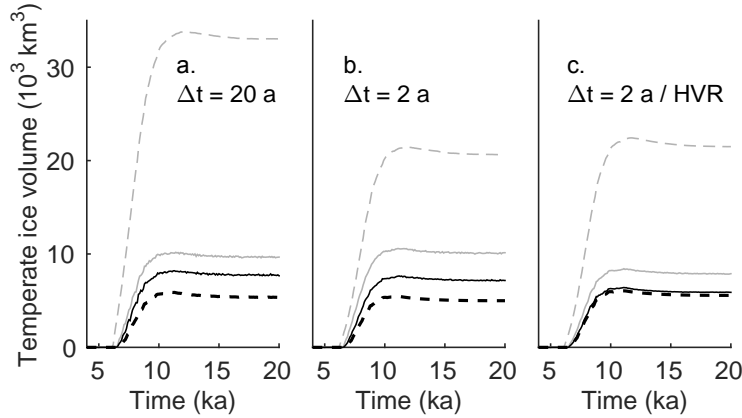


Figure 3: EISMINT experiment A1: Evolution of the temperate ice volume over the first 20 ka model time. Black dashed: POLY scheme, gray dashed: COLD scheme, gray solid: ENTC scheme, black solid: ENTM scheme (see Sect. 3 for the scheme codes). Grid resolution $\Delta x = 10$ km. a: Time step $\Delta t = 20$ a. b: Time step $\Delta t = 2$ a. c: Time step $\Delta t = 2$ a, high vertical resolution (see Sect. 4 for details).

then converges towards a steady-state value. The main difference between the larger (20 a, panel a) and the smaller (2 a, panel b) time step is the behaviour of the COLD scheme. Compared to the POLY scheme, for $\Delta t = 20$ a it overpredicts the temperate ice volume by more than a factor 6, while for $\Delta t = 2$ a the overprediction factor is ~ 4 . The results of the POLY, ENTM and ENTC schemes do not change much; ENTC produces $\sim 2\times$ more and ENTM $\sim 1.4\times$ more temperate ice than POLY. Employing the high vertical resolution (panel c) reduces the discrepancy between the POLY and ENTM schemes to less than 10%, and the overprediction by the ENTC scheme to a factor ~ 1.4 , while there is little influence on the poor performance of the COLD scheme.

For both time steps and the standard vertical resolution (panels a, b), the ENTC and ENTM schemes show some high-frequency noise in the evolution of the temperate ice volume (amplitudes less than 2% of the total temperate ice volume), while the results produced by the POLY scheme and the COLD scheme are smoother. The noisiness is clearly reduced (but still visible) for the high vertical resolution (panel c). This makes the one-layer approach of ENTC and ENTM, with its positioning of the CTS at a discrete grid point (uppermost grid point of the temperate layer, see Sects. 3.3 and 3.4)

a likely cause. However, the one-dimensional simulations carried out by Blatter and Greve (2015) for a parallel-sided slab did not show any noise, so that its occurrence is also related to the three-dimensionality of the problem considered here (see below).

Figures 4-6 show maps of the steady-state thickness of the temperate layer for experiment A1, all four thermodynamics solvers and the same set-ups as in Fig. 3. The decreasing amount of temperate ice in the order COLD > ENTC > ENTM > POLY is clearly visible. The larger time step in Fig. 4 compared to Fig. 5 mainly affects the results of the POLY and COLD schemes. For the COLD scheme, this was already discussed above. For the POLY scheme, a numerical instability occurs in the form of a waviness of the thickness of the temperate layer oriented diagonally to the x - and y -axes. The smaller time step used in Fig. 5 resolves this problem.

The larger temporal noise produced by the two enthalpy schemes (as discussed above) finds its counterpart in larger spatial noise (compare the respective panels c and d to a and b). The two types of noise are strongly related to each other. Both are largely unaffected by the time step (Fig. 5 vs. Fig. 4), but significantly reduced by the higher vertical resolution (Fig. 6 vs. Fig. 5). For the small-time-step/high-vertical-resolution set-up used in Fig. 6, the results of the POLY and ENTM schemes are very similar to each other.

Further, in all cases, the thickness of the temperate layer tends to increase gradually with distance from the center of the ice sheet, and then decreases sharply near the ice margin. This confirms for our new simulations what was already claimed in Sect. 1, and it is the reason for the fact that freezing conditions at the CTS can hardly be resolved, thus justifying that we ignored them for this study. Owing to the incompatible symmetries of the ice sheet geometry (circularly symmetric) and the numerical grid (aligned to the x - and y -axes), the thin rings of largest temperate layer thicknesses near the margin are in all cases somewhat discontinuous.

A synopsis of the main results of the 16 set-ups of experiment A1 (all set-ups shown in Figs. 3-6, plus the high-horizontal-resolution case $\Delta x = 5$ km, $\Delta t = 2$ a) is given in Table 1. The volume of temperate ice is in the range of ~ 0.25 - 1% of the total ice volume and, as discussed above, varies strongly across the different thermodynamics schemes. By contrast, the melt fraction (area ratio of basal temperate ice to total ice) is much larger ($\sim 2/3$) and varies very little across all 16 set-ups. For the total ice volume and area, the strongest systematic (but still small) influence arises from the horizontal

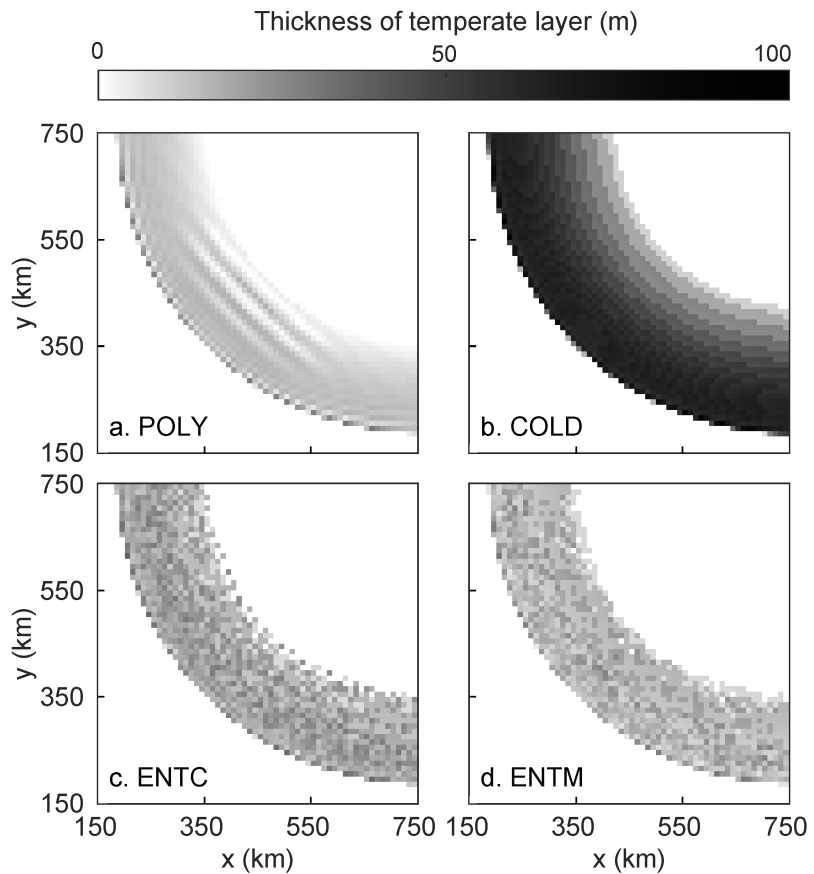


Figure 4: EISMINT experiment A1: Thickness of the basal temperate ice layer after 200 ka model time. a: POLY scheme, b: COLD scheme, c: ENTC scheme, d: ENTM scheme (see Sect. 3 for the scheme codes). Grid resolution $\Delta x = 10$ km, time step $\Delta t = 20$ a.

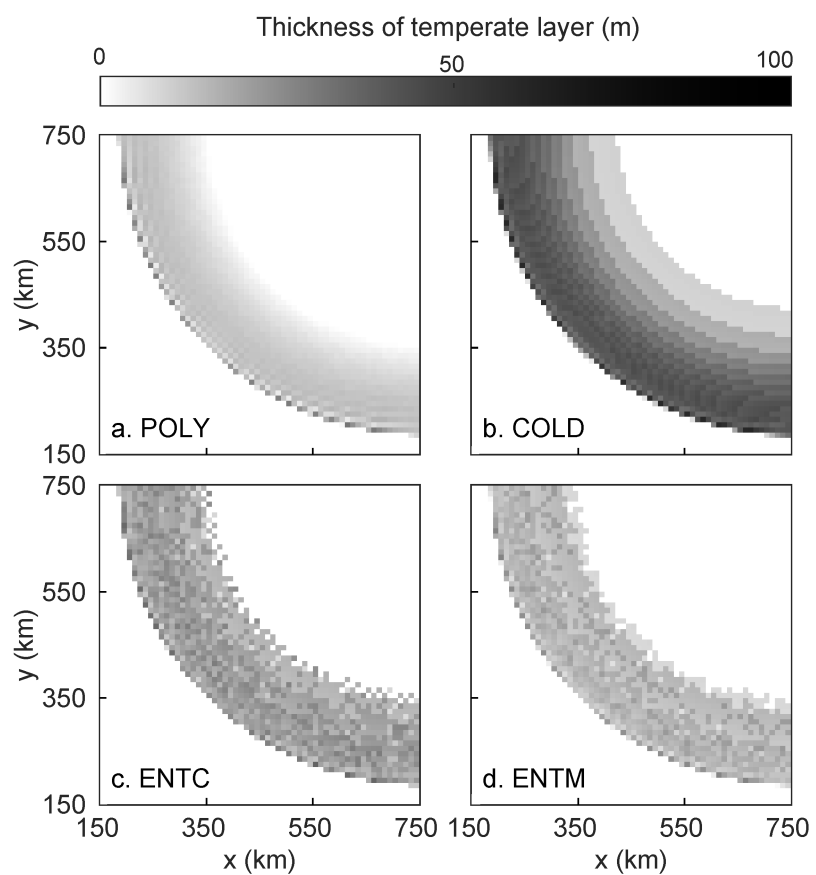


Figure 5: Same as Fig. 4, but grid resolution $\Delta x = 10$ km, time step $\Delta t = 2$ a.

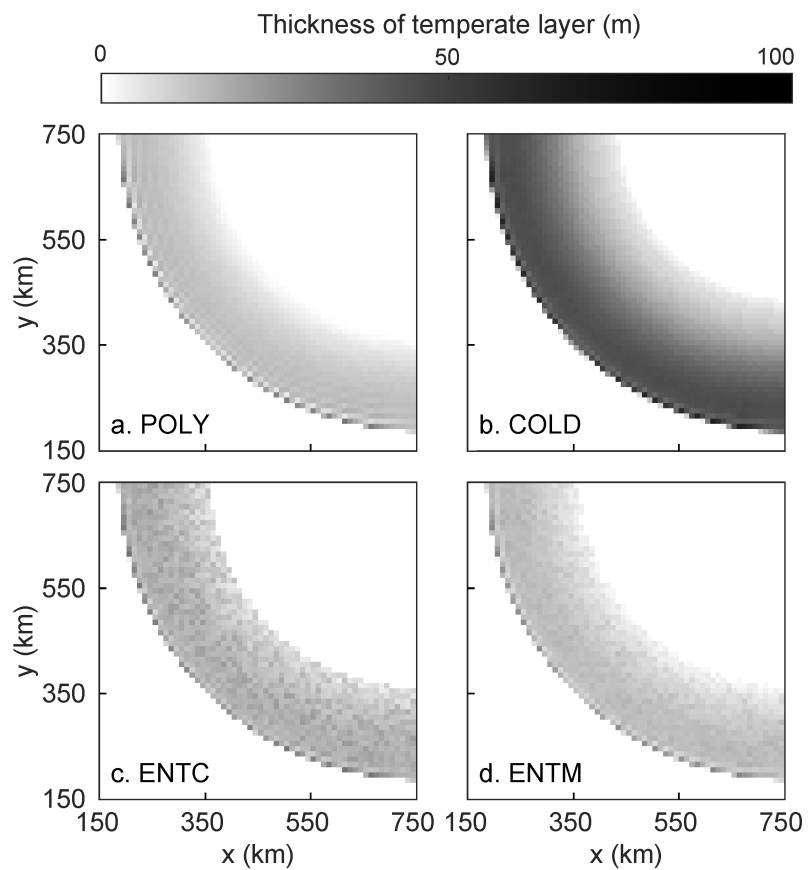


Figure 6: Same as Fig. 4, but grid resolution $\Delta x = 10$ km, time step $\Delta t = 2$ a, high vertical resolution (see Sect. 4 for details).

Exp. A1 set-up (scheme, Δx , Δt)	Volume (10^6 km^3)	Area (10^6 km^2)	Temp. volume (10^4 km^3)	Melt fraction
POLY, 10 km, 20 a	2.105	1.045	0.537	0.675
COLD, 10 km, 20 a	2.109	1.043	3.319	0.671
ENTC, 10 km, 20 a	2.097	1.044	0.968	0.673
ENTM, 10 km, 20 a	2.113	1.046	0.775	0.674
POLY, 10 km, 2 a	2.109	1.046	0.501	0.675
COLD, 10 km, 2 a	2.120	1.044	2.076	0.675
ENTC, 10 km, 2 a	2.096	1.044	1.008	0.676
ENTM, 10 km, 2 a	2.110	1.046	0.718	0.674
POLY, 5 km, 2 a	2.123	1.050	0.466	0.675
COLD, 5 km, 2 a	2.133	1.049	2.009	0.674
ENTC, 5 km, 2 a	2.110	1.050	0.977	0.675
ENTM, 5 km, 2 a	2.124	1.050	0.689	0.675
POLY, 10 km, 2 a (hvr)	2.105	1.045	0.559	0.695
COLD, 10 km, 2 a (hvr)	2.120	1.044	2.159	0.696
ENTC, 10 km, 2 a (hvr)	2.101	1.044	0.790	0.694
ENTM, 10 km, 2 a (hvr)	2.105	1.045	0.595	0.694

Table 1: EISMINT experiment A1: Mean values between $t = 190 \text{ ka}$ and 200 ka for the ice volume, the ice area, the volume of temperate ice and the melt fraction (fraction of basal ice at the pressure melting point). See Sect. 3 for the scheme codes. The abbreviation “hvr” means “high vertical resolution” (see Sect. 4 for details).

Exp. A1 set-up (scheme, Δx , Δt)	Computing time (hrs)
POLY, 10 km, 2 a	7.7
COLD, 10 km, 2 a	4.2
ENTC, 10 km, 2 a	7.0
ENTM, 10 km, 2 a	8.2

Table 2: Computing times for EISMINT experiment A1 with the reference set-up ($\Delta x = 10 \text{ km}$, $\Delta t = 2 \text{ a}$), run with the Intel Fortran Compiler 15.0.3 for Linux (optimization options `-xHOST -O3 -no-prec-div`) on a 12-Core Intel Xeon E5-2697 v2 (2.7 GHz) PC under openSUSE 13.1 (64 bit). See Sect. 3 for the scheme codes.

resolution: On average, $\Delta x = 5$ km produces an ice sheet with 0.7% more volume and 0.5% more area than $\Delta x = 10$ km. By contrast, the influences of the thermodynamics solver, the time step and the vertical resolution are unsystematic and even smaller.

In Table 2, the computing times of the four thermodynamics schemes are compared for Experiment A1 with $\Delta x = 10$ km and $\Delta t = 2$ a. The differences between the schemes are significant. As expected, the most simple, but physically inadequate COLD scheme is by far the fastest, with a gain of more than 40% compared to the POLY scheme. The differences between the POLY, ENTM and ENTC schemes are smaller. ENTC is about 10% faster than POLY, while ENTM is about 6% slower. The reason for the relative slowness of the enthalpy schemes, despite greater simplicity compared to the POLY scheme, is that, in the SICOPOLIS implementation, in each time step the computed enthalpy field is converted back to temperature and water content. This must be done three-dimensionally and is thus costly. Codes that are designed as enthalpy-based from the outset (whereas the thermodynamics of SICOPOLIS is natively based on temperature and water content) can probably avoid these conversions, which opens the possibility for greater efficiency of the enthalpy schemes.

For experiment A2, the water-content-dependent rate factor for temperate ice has been replaced by a constant rate factor like in the original EISMINT set-up (Sect. 4.2). The resulting steady-state thickness of the temperate layer for all four thermodynamics solvers and the combination $\Delta x = 10$ km, $\Delta t = 2$ a is shown in Fig. 7, and an overview of the main results is given in Table 3. The COLD scheme is unaffected by the difference between experiments A1 and A2 because it does not account for any water content, and consequently the results are the same. By contrast, the POLY, ENTM and ENTC schemes produce roughly two times thicker temperate ice layers for experiment A2. The reason is that the simulated temperate ice is stiffer, which reduces the advective transport of cold ice towards the base, so that the growth of the temperate ice layers is favoured compared to experiment A1. It is interesting to note that, for experiment A2, the temperate ice volumes computed by the POLY and ENTM schemes agree very well (within 3%) for the standard vertical resolution employed here. For experiment A1, a similarly close agreement is only achieved with the high vertical resolution (see discussion above).

There is no notable influence of experiment A2 on the melt fraction. The total ice area is essentially unaffected as well, while the total ice volume is

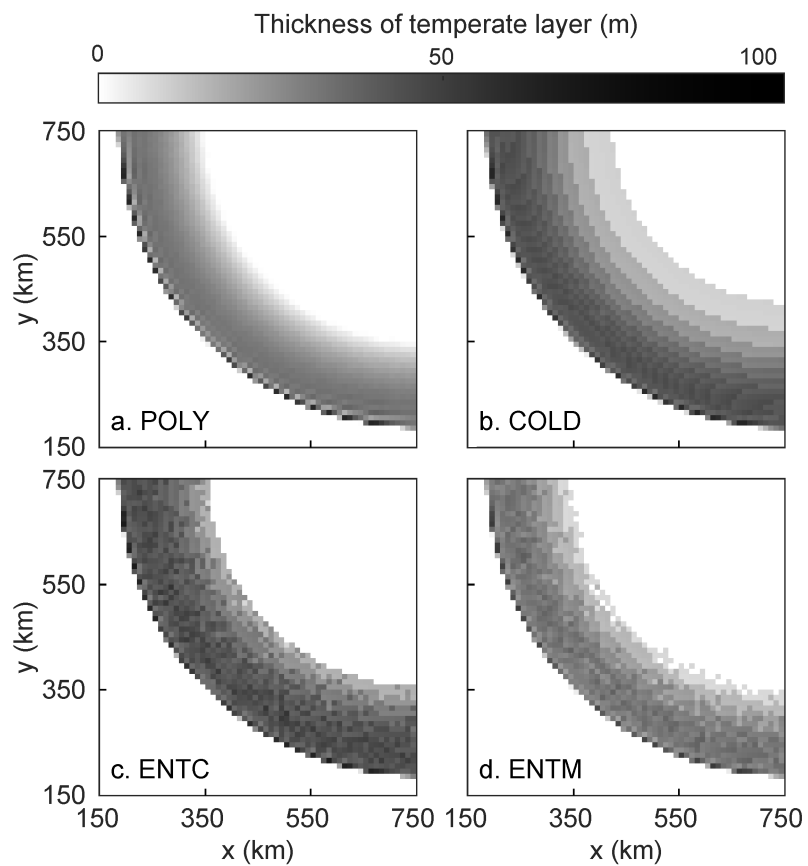


Figure 7: Same as Fig. 4, but for EISMINT experiment A2, grid resolution $\Delta x = 10$ km, time step $\Delta t = 2$ a.

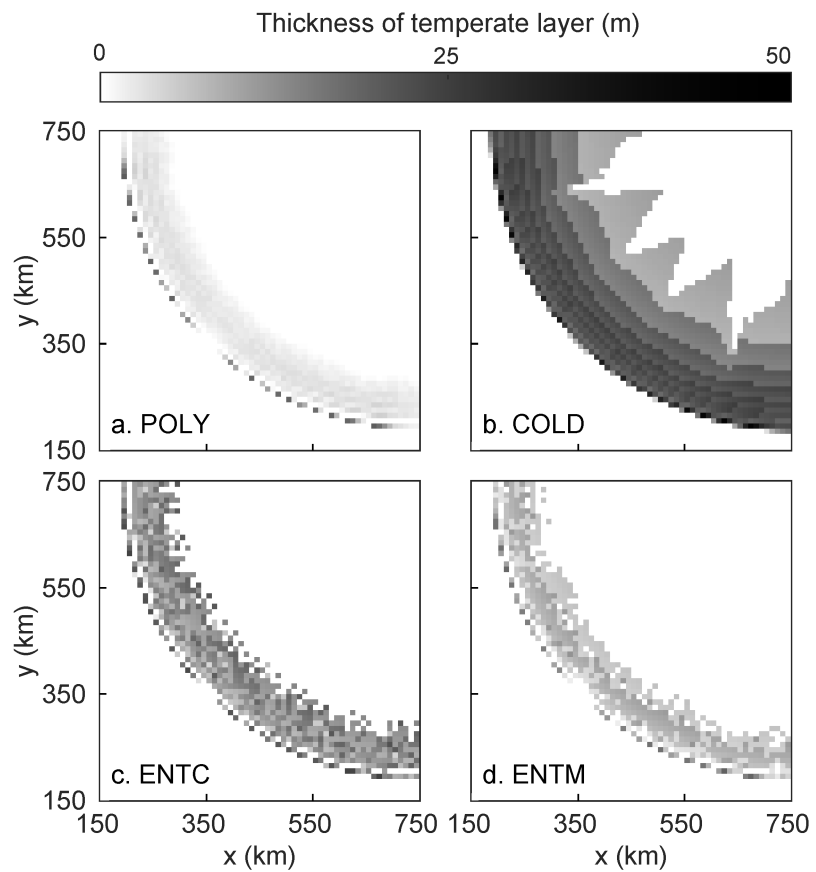


Figure 8: Same as Fig. 4, but for EISMINT experiment H1, grid resolution $\Delta x = 10$ km, time step $\Delta t = 2$ a.

Exp. A1 set-up (scheme, Δx , Δt)	Volume (10^6 km^3)	Area (10^6 km^2)	Temp. volume (10^4 km^3)	Melt fraction
POLY, 10 km, 2 a	2.109	1.046	0.501	0.675
COLD, 10 km, 2 a	2.120	1.044	2.076	0.675
ENTC, 10 km, 2 a	2.096	1.044	1.008	0.676
ENTM, 10 km, 2 a	2.110	1.046	0.718	0.674
Exp. A2 set-up (scheme, Δx , Δt)	Volume (10^6 km^3)	Area (10^6 km^2)	Temp. volume (10^4 km^3)	Melt fraction
POLY, 10 km, 2 a	2.124	1.044	1.245	0.675
COLD, 10 km, 2 a	2.120	1.044	2.076	0.675
ENTC, 10 km, 2 a	2.120	1.044	1.956	0.675
ENTM, 10 km, 2 a	2.123	1.044	1.273	0.676
Exp. H1 set-up (scheme, Δx , Δt)	Volume (10^6 km^3)	Area (10^6 km^2)	Temp. volume (10^4 km^3)	Melt fraction
POLY, 10 km, 2 a	2.094	1.045	0.079	0.668
COLD, 10 km, 2 a	2.090	1.041	1.149	0.659
ENTC, 10 km, 2 a	2.087	1.045	0.365	0.664
ENTM, 10 km, 2 a	2.096	1.045	0.176	0.664

Table 3: EISMINT experiments A1, A2 and H1: Mean values between $t = 190 \text{ ka}$ and 200 ka for the ice volume, the ice area, the volume of temperate ice and the melt fraction (fraction of basal ice at the pressure melting point). See Sect. 3 for the scheme codes.

systematically slightly (on average $\sim 0.8\%$) larger than in experiment A1.

For experiment H1, basal sliding over temperate- and near-temperate-based areas has been added to the set-up of experiment A1 (Sect. 4.3). Like for experiment A2, we only discuss the combination $\Delta x = 10 \text{ km}$, $\Delta t = 2 \text{ a}$. Figure 8 depicts the steady-state thickness of the temperate layer for the four thermodynamics solvers, and Table 3 gives an overview of the results. Comparing Figs. 5 and 8 as well as the entries in Table 3 reveals that the addition of some basal sliding reduces the volume of temperate ice strongly. This is a consequence of increased advection of cold surface ice downward and outward, and of reduced strain heating. Like for experiments A1 and A2, the computed temperate ice volume decreases in the order COLD > ENTC > ENTM > POLY. However, even the ENTM scheme overpredicts the temperate ice volume by more than a factor 2 compared to the POLY scheme. This is because the thicknesses are so small that any one-layer scheme does not resolve them well (unless a very high vertical resolution is

employed), whereas the performance of the two-layer POLY scheme is not limited by this problem.

Figure 8b shows further that in the distribution of temperate ice obtained with the COLD scheme some spokes emerge. The spokes are also present in similar form in the results of the three other schemes when the basal temperature is plotted instead of the thickness of the temperate ice layer (not shown). This phenomenon was already observed in the original article on the EISMINT Phase 2 Simplified Geometry Experiments (Payne and others, 2000). It is most likely a consequence of the combined effects of a thermo-viscous flow instability and the symmetry of the numerical grid (Bueler and others, 2007).

Since the sliding coefficient in experiment H1 is small, the melt fraction and the total ice volume only decrease slightly compared to those of experiment A1, and the ice area is virtually unchanged. This underlines the very high sensitivity of the temperate ice layer to changed flow conditions. For the original experiment H with a 10 times larger sliding coefficient (results not shown), the large-scale response of the ice sheet is more pronounced. For this scenario, only the COLD scheme produces a temperate layer of non-zero thickness, while the other schemes merely produce a temperate base.

6. Discussion and conclusion

We tested four different thermodynamics solvers in the ice sheet model SICOPOLIS. Two of them are the previously existing polythermal two-layer (POLY) and cold-ice (COLD) schemes, while the other two are the newly implemented conventional one-layer enthalpy (ENTC) and melting-CTS one-layer enthalpy (ENTM) schemes. The ENTC scheme goes back to the study by Aschwanden and others (2012), while the ENTM scheme was introduced by Blatter and Greve (2015) for a one-dimensional ice slab. Extension to the full, three-dimensional problem was straightforward because, due to the neglect of horizontal diffusive heat fluxes, the computation of the thermodynamic fields (temperature and water content or enthalpy) is essentially one-dimensional for each column. Horizontal advection merely plays the role of an additional source term for the vertical profiles and does not constitute a problem for the implementation of the scheme.

We used two scenarios from the suite of EISMINT (European Ice Sheet Modeling INiTiative) Phase 2 Simplified Geometry Experiments (Payne and others, 2000) as our model problems, one without and one with basal sliding.

Like in the one-dimensional study carried out by Blatter and Greve (2015), the results computed with the POLY scheme were assessed to be most reliable and thus chosen as a reference.

As it was already reported by Greve (1997b), the COLD scheme strongly overpredicts thicknesses of temperate ice layers, and thus temperate ice volumes. Choosing a small time step reduces the amount of overprediction to a certain extent, but the performance of the COLD scheme (which is not energy-conserving and thus physically incorrect anyway) is not satisfactory.

The studies by Kleiner and others (2015) and Blatter and Greve (2015), both carried out for a Canadian-type parallel-sided slab, found that the ENTC scheme, even though it does not enforce the transition conditions at the CTS explicitly, still fulfills them for the case of melting conditions (continuity of the enthalpy and the sensible heat flux), provided that the discontinuity of the enthalpy diffusivity (11) at the CTS is properly accounted for in the discretization of the diffusion term in the enthalpy equation (10). This could not be confirmed in the present study: even though the ENTC scheme has been implemented in SICOPOLIS in the same way as described by Blatter and Greve (2015), the scheme fails to produce a continuous temperature gradient across the CTS and overpredicts temperate ice layer thicknesses, albeit to a smaller degree than the COLD scheme (always compared to the references provided by the POLY scheme). We speculate that this is a consequence of the three-dimensionality of the problem investigated here, most likely due to the additional horizontal advection terms in the enthalpy equation.

In contrast to the ENTC scheme, the continuity of the temperature gradient across the CTS is explicitly enforced by the ENTM scheme. This leads to a better match of computed temperate ice layer thicknesses to those computed by the POLY scheme; however, some overprediction remains. The price to pay for enforcing a continuous temperature gradient across the CTS, while the positioning of the CTS is limited by the grid resolution, is a slight discontinuity of the ice temperature itself.

When comparing the temperature profiles in the ice column above the CTS, the ENTC and ENTM schemes perform both well compared to the POLY scheme, while the temperatures produced by the COLD scheme are too high. The water content in the temperate ice layer below the CTS usually reaches the threshold value of 0.01 (1%) for the POLY, ENTC and ENTM schemes, while the COLD scheme does not compute any water content.

The ENTC and ENTM schemes produce some temporal and spatial noise

for the volume and thickness of the temperate ice. This does not happen for the POLY and COLD schemes; it is related to the one-layer approach in which we position the CTS at the uppermost grid point in the temperate layer, whereas the POLY scheme allows, in principle, tracking the position of the CTS to arbitrary accuracy. A possible improvement of the one-layer enthalpy schemes would be to implement a sub-grid tracking of the CTS position, which would likely allow to fulfill the continuity of the temperate and of the temperature gradient across the CTS simultaneously and reduce the noise. However, such a sub-grid tracking scheme will inevitably increase the computational cost.

To sum up, for a polythermal ice sheet model, the one-layer enthalpy schemes ENTC and ENTM are viable, easier implementable alternatives to the POLY scheme with its slightly awkward need to handle two different numerical domains for cold and temperate ice. ENTM is more precise than ENTC for determining the position of the CTS, and thus the volume and thickness of the temperate ice layer. The performance of both schemes is good for the temperature profiles in the cold ice column above the CTS and also the water content in the temperate ice layer below the CTS. The computing times of all three schemes are comparable.

Acknowledgements

We thank the two anonymous reviewers and the scientific editor, T. Kameda, for their comments that helped considerably to improve the manuscript. R.G. was supported by the Japanese Ministry of Education, Culture, Sports, Science and Technology (MEXT) through the Green Network of Excellence (GREENE) Arctic Climate Change Research project and the Arctic Challenge for Sustainability (ArCS) project. H.B. was supported by an Invitation Fellowship for Research in Japan (No. L13525) of the Japan Society for the Promotion of Science (JSPS).

References

Aschwanden, A., E. Bueler, C. Khroulev and H. Blatter, 2012. An enthalpy formulation for glaciers and ice sheets, *J. Glaciol.*, **58**(209), 441–457.

Blatter, H. and R. Greve, 2015. Comparison and verification of enthalpy schemes for polythermal glaciers and ice sheets with a one-dimensional model, *Polar Sci.*, **9**(2), 196–207.

Blatter, H. and K. Hutter, 1991. Polythermal conditions in Arctic glaciers, *J. Glaciol.*, **37**(126), 261–269.

Brinkerhoff, D. J. and J. V. Johnson, 2013. Data assimilation and prognostic whole ice sheet modelling with the variationally derived, higher order, open source, and fully parallel ice sheet model VarGlaS, *Cryosphere*, **7**(4), 1161–1184.

Bueller, E. and J. Brown, 2009. Shallow shelf approximation as a “sliding law” in a thermomechanically coupled ice sheet model, *J. Geophys. Res. Earth Surf.*, **114**(F3), F03008.

Bueller, E., J. Brown and C. Lingle, 2007. Exact solutions to the thermomechanically coupled shallow ice approximation: effective tools for verification, *J. Glaciol.*, **53**(182), 499–516.

Calov, R. and K. Hutter, 1996. The thermomechanical response of the Greenland ice sheet to various climate scenarios, *Clim. Dynam.*, **12**(4), 243–260.

Gilbert, A., O. Gagliardini, C. Vincent and P. Wagnon, 2014. A 3-D thermal regime model suitable for cold accumulation zones of polythermal mountain glaciers, *J. Geophys. Res. Earth Surf.*, **119**(9), 1876–1893.

Golledge, N. R., R. H. Levy, R. M. McKay, C. J. Fogwill, D. A. White, A. G. C. Graham, J. A. Smith, C.-D. Hillenbrand, K. J. Licht, G. H. Denton, R. P. Ackert, Jr., S. M. Maas and B. L. Hall, 2013. Glaciology and geological signature of the Last Glacial Maximum Antarctic ice sheet, *Quaternary Sci. Rev.*, **78**, 225–247.

Greve, R., 1997a. A continuum-mechanical formulation for shallow polythermal ice sheets, *Phil. Trans. R. Soc. Lond. A*, **355**(1726), 921–974.

Greve, R., 1997b. Application of a polythermal three-dimensional ice sheet model to the Greenland ice sheet: Response to steady-state and transient climate scenarios, *J. Climate*, **10**(5), 901–918.

Greve, R., 2005. Relation of measured basal temperatures and the spatial distribution of the geothermal heat flux for the Greenland ice sheet, *Ann. Glaciol.*, **42**, 424–432.

Greve, R. and H. Blatter, 2009. Dynamics of Ice Sheets and Glaciers, Springer, Berlin, Germany etc.

Greve, R. and U. C. Herzfeld, 2013. Resolution of ice streams and outlet glaciers in large-scale simulations of the Greenland ice sheet, *Ann. Glaciol.*, **54**(63), 209–220.

Hindmarsh, R. C. A. and E. Le Meur, 2001. Dynamical processes involved in the retreat of marine ice sheets, *J. Glaciol.*, **47**(157), 271–282.

Hooke, R. LeB., 2005. Principles of Glacier Mechanics, Cambridge University Press, Cambridge, UK and New York, NY, USA, 2nd ed.

Huybrechts, P., 1990. A 3-D model for the Antarctic ice sheet: a sensitivity study on the glacial-interglacial contrast, *Clim. Dynam.*, **5**, 79–92.

Kleiner, T., M. Rückamp, J. Bondzio and A. Humbert, 2015. Enthalpy benchmark experiments for numerical ice sheet models, *Cryosphere*, **9**(1), 217–228.

Lliboutry, L. and P. Duval, 1985. Various isotropic and anisotropic ices found in glaciers and polar ice caps and their corresponding rheologies, *Ann. Geophys.*, **3**(2), 207–224.

Payne, A. J. and P. W. Dongelmans, 1997. Self-organization in the thermomechanical flow of ice sheets, *J. Geophys. Res. Solid Earth*, **102**(B6), 12219–12233.

Payne, A. J., P. Huybrechts, A. Abe-Ouchi, R. Calov, J. L. Fastook, R. Greve, S. J. Marshall, I. Marsiat, C. Ritz, L. Tarasov and M. P. A. Thomassen, 2000. Results from the EISMINT model intercomparison: the effects of thermomechanical coupling, *J. Glaciol.*, **46**(153), 227–238.

Pettersson, R., P. Jansson, H. Huwald and H. Blatter, 2007. Spatial pattern and stability of the cold surface layer of Storglaciären, Sweden, *J. Glaciol.*, **53**(180), 99–109.

Ritz, C., A. Fabré and A. Letréguilly, 1997. Sensitivity of a Greenland ice sheet model to ice flow and ablation parameters: consequences for the evolution through the last climatic cycle, *Clim. Dynam.*, **13**(1), 11–24.

Sato, T. and R. Greve, 2012. Sensitivity experiments for the Antarctic ice sheet with varied sub-ice-shelf melting rates, *Ann. Glaciol.*, **53**(60), 221–228.

Seroussi, H., M. Morlighem, E. Rignot, A. Khazendar, E. Larour and J. Mouginot, 2013. Dependence of century-scale projections of the Greenland ice sheet on its thermal regime, *J. Glaciol.*, **59**(218), 1024–1034.

Wilson, N. J. and G. E. Flowers, 2013. Environmental controls on the thermal structure of alpine glaciers, *Cryosphere*, **7**(1), 167–182.